

Micro/Nanoscale Mechanical and Tribological Characterization of SiC for Orthopedic Applications

Xiaodong Li,¹ Xinnan Wang,¹ Robert Bondokov,² Julie Morris,² Yuehuei H. An,³ Tangali S. Sudarshan²

¹ Department of Mechanical Engineering, University of South Carolina, 300 Main Street, Columbia, South Carolina 29208

² Department of Electrical Engineering, University of South Carolina, 301 Main Street, Columbia, South Carolina 29208

³ Orthopaedic Research Laboratory, Medical University of South Carolina, 96 Jonathan Lucas Street, CSB708, Charleston, South Carolina 29425

Received 6 May 2004; revised 21 July 2004; accepted 2 August 2004

Published online 10 November 2004 in Wiley InterScience (www.interscience.wiley.com). DOI: 10.1002/jbm.b.30168

Abstract: Micro/nanomechanical and tribological characterization of SiC has been carried out. For comparison, measurements on SiC, CoCrMo, Ti-6Al-4V, and stainless steel have also been made. Hardness and elastic modulus of these materials were measured by nanoindentation using a nanoindenter. The nanoindentation impressions were imaged using an atomic force microscope (AFM). Scratch, friction, and wear properties were measured using an accelerated microtribometer. Scratch and wear damages were studied using a scanning electron microscope (SEM). It is found that SiC exhibits higher hardness, elastic modulus, scratch resistance as well as lower friction with fewer and smaller debris particles compared to other materials. These results show that SiC possesses superior mechanical and tribological properties that make it an ideal material for use in orthopedic and other biomedical applications. © 2004 Wiley Periodicals, Inc. *J Biomed Mater Res Part B: Appl Biomater* 72B: 353–361, 2005

Keywords: SiC; biomaterials; orthopedic; nanoindentation; mechanical properties; tribology

INTRODUCTION

Silicon carbide (SiC) has great potential for overcoming the current inadequacies of orthopedic materials due to its inherent characteristic of being chemically inert and consequently resistant to harsh mechanical and chemical environments. While initial research has been performed on SiC for implantation and biocompatibility, including as a coating in orthopedics for the prosthetic-bearing surface and the uncemented joint prosthetic, and SiC is currently in clinical use as a coating for stents to enhance hemocompatibility,^{1–8} SiC has not undergone the focused and comprehensive studies necessary to make it an accepted alternative to current orthopedic materials. Due to the inertness of SiC, this material would become permanently integrated into the new bone growth without the disadvantages of wear debris generation, oxidation, and metallosis that generally occur with implanted ma-

terials. Prior to its development as an implant, SiC must be thoroughly evaluated to establish its safety for implantation and its material characteristics as compared to current materials. Once its advantages to current materials are demonstrated, further studies can be undertaken to proceed with the development of the scaffold structures ultimately leading to clinical trials with the new material.

The major disadvantage with traditional orthopedic materials used for joint replacement, such as titanium, cobalt chrome, and stainless steel, is their propensity to wear. The particles produced as wear debris lead to bone loss and implant loosening.⁹ Due to this, prostheses may need to be replaced every 10 to 15 years. Additionally, these materials oxidize over time creating a reactive implant surface, as well as local and systemic metallosis. Solid surfaces, such as metal implants, allow different levels of natural integration with bone or other tissues in the body, based on the degree of biocompatibility of the implants.¹⁰ Thus, a new mechanically stable material that lasts longer, generates less wear, invites better tissue growth, and is stable and biocompatible would be a great advancement to this field. In addition, joint replacement surgery in children and young adults less than 30 is generally only reserved for patients with significant debilitation due to a greater risk of complications, such as increased implant wear and shorter implant life spans, even

Correspondence to: X. Li, Department of Mechanical Engineering, University of South Carolina, 300 Main Street, Columbia, SC 29208 (e-mail: lixiao@enr.sc.edu)

Contract grant sponsor: National Science Foundation; contract grant number: EPS-0296165

Contract grant sponsor: University of South Carolina Research Foundation Equipment Grant Award

Contract grant sponsor: University of South Carolina VPR Opportunity funds

Contract grant sponsor: University of South Carolina NanoCenter

TABLE I. Mechanical and Tribological Properties of SiC, CoCrMo, Ti-6Al-4V, and Stainless Steel

Material	Hardness (GPa)	Elastic modulus (GPa)	Critical load (mN)	Wear Coefficient of Friction		Particle Size (μm)	Damage Index
				Beginning	End		
SiC	45.8	370	27	0.17	0.2	0.4	1
CoCrMo	10.1	300	13	0.17	0.23	1.3	2
Ti-6Al-4V	5.6	127	12	0.23	0.26	7.9	4
Stainless steel	6.2	223	9	0.45	0.40	8.1	3

though they may experience substantial pain or activity loss.^{9,11} Ideally, orthopedic devices should meet the load-bearing and movement requirements of an active population with an extended material lifetime devoid of degradation.¹²

The continuous research on implantable biomaterials for use in orthopedic surgery is due to the limitations of the currently available biomaterials. As described above, periprosthetic osteolysis are caused by the generation of wear debris by current orthopedic biomaterials.^{13,14} In contrast, SiC possesses all of the properties lacking in the above situations: mechanical strength, superior biocompatibility, and an anti-abrasive nature.

SiC is expected to possess superior biocompatibility properties because it is chemically inert and exhibits properties that may indicate improved mechanical characteristics such as wear and hardness compared with standard orthopedic materials.^{5,15–17} There has been a variety of research performed on SiC for implantation and biocompatibility, including as a coating in orthopedics for the prosthetic-bearing surface and the uncemented joint prosthetic, and SiC is currently in clinical use as a coating for stents to enhance hemocompatibility.^{1–8} One study shows that SiC particles were well tolerated by rabbit bone, did not cause aggregation of macrophages, and were apparently harmless. This study found SiC particulate matter to be safe, and a possible stimulant of bone in-growth.¹ Despite the promising characteristics of this material as demonstrated from this research, few facilities have the capabilities to fabricate and further develop the material for orthopedic applications.

Reliability studies are the key for practical application and commercialization of today's advanced biomaterials. Mechanical and tribological aspects are of critical importance in determining long-term stability of medical implants and devices. Aseptic loosening of total joint replacements begins as a mechanical problem, which is initiated by joint articulation and other relative motion between surfaces. Wear debris can cause calcar resorption and implant loosening. Debris generated as a result invokes biological responses that accelerate loosening by propelling changes in the bone. One of the crucial factors is the release of wear debris particles that initiate the inflammatory cascade. An in-depth understanding of the mechanical and tribological properties of biomaterials is therefore fundamental to the control of fracture failure and wear in new implants.

The objectives of this study were to identify a new orthopedic material, SiC, that exhibits superior mechanical and

tribological properties, and to understand failure mechanisms of current orthopedic materials. Nanoindentation, micro-scratch, and wear experiments were conducted using a nanoindenter and a microtribometer. Indentation, scratch, and wear damage mechanisms were analyzed by atomic force microscopy (AFM) and scanning electron microscopy (SEM).

EXPERIMENTAL

Test Samples

Silicon carbide bulk crystals were grown using the seeded physical vapor transport (PVT) technique.¹⁸ In this method, SiC powder is used as a source and heated to 2500°C, resulting in extensive sublimation. The SiC species are then transported by diffusion to the seed on which SiC material crystallizes into bulk. Conventional PVT technique is the only method used to grow large diameter SiC single crystals suitable for electronic devices. This method allows control of the growth parameters, such as growth rate, thermal gradient, seeding, etc., that is used to produce SiC material with predictable crystallinity, polytype, doping concentration, etc.

6H-SiC bulk crystals were grown under the following conditions: The temperature of the seed was varied between 1900°C and 2300°C, controlled by a pyrometer. Resistive heating, as well as radiofrequency-heating furnaces, were used with the temperature gradient $\leq 30^\circ\text{C}/\text{cm}$ between the source and seed. The argon background pressure was maintained between 1 and 50 Torr. The grown SiC single crystals were oriented using Xray diffractometer and sliced into wafers using a wire saw. The wafers were then lapped and polished to obtain a smooth surface ($\text{RMS} \leq 5 \text{ \AA}$) and to perform the necessary studies. Finally, the SiC samples were cleaned using standard procedures including an ultrasonic bath.

Three commonly used orthopedic biomaterials were tested along with SiC, including cobalt-chromium-molybdenum (CoCrMo), titanium-6 aluminum-4 vanadium alloy, and (Ti-6Al-4V), stainless steel 316L (SS 316L) (ASTM F138) were kindly provided by Oncore Orthopaedics (Austin, TX). They were machined from metal bars into disks measuring 12.0 mm in diameter and 2.5 mm in thickness. Before testing, the surfaces of the disks were hand polished using a series of

silicon carbide metallographic papers down to a grit size of 1200. Properties of the materials tested are listed in Table I.

Mechanical and Tribological Characterization

Nanoindentation tests were performed using a Troboscope nanomechanical testing system (Hysitron Inc.) in conjunction with a Veeco Dimension 3100 AFM system (Veeco Metrology Group). The Hysitron nanoindenter monitors and records the load and displacement of the indenter, a diamond Berkovich three-sided pyramid, with a force resolution of about 1 nN and displacement resolution of about 0.1 nm. Hardness and elastic modulus were calculated from the recorded load–displacement curves. The indentation impressions were then imaged *in situ* using the indenter tip. A series of 10 indentations were performed for each sample.

Nanoindentation hardness is defined as the indentation load divided by the projected contact area of the indentation. It is the mean pressure that a material will support under load. From the load–displacement curve, hardness can be obtained at the peak load as

$$H = \frac{P_{\max}}{A} \quad (1)$$

where P_{\max} is the peak load and A is the projected contact area. For an indenter with a known geometry such as the Berkovich tip used in this study, the projected contact area is a function of contact depth, which is measured by the nanoindenter *in situ* during indentation.^{19–21} Therefore, the projected area A can be measured and calculated directly from the indentation displacement.

The elastic modulus was calculated using the Oliver–Pharr data analysis procedure²² beginning by fitting the unloading curve to a power–law relation. The unloading stiffness can be obtained from the slope of the initial portion of the unloading curve, $S = dP/dh$. Based on relationships developed by Sneddon²³ for the indentation of an elastic half space by any punch that can be described as a solid of revolution of a smooth function, a geometry-independent relation involving contact stiffness, contact area, and elastic modulus can be derived as follows:

$$S = 2\beta \sqrt{\frac{A}{\pi}} E_r \quad (2)$$

where β is a constant which depends on the geometry of the indenter ($\beta = 1.034$ for a Berkovich indenter),^{19–21} and E_r is the reduced elastic modulus which accounts for the fact that elastic deformation occurs in both the sample and the indenter. E_r is given by

$$\frac{1}{E_r} = \frac{1 - \nu^2}{E} + \frac{1 - \nu_i^2}{E_i} \quad (3)$$

where E and ν are the elastic modulus and Poisson's ratio for the sample, and E_i and ν_i are the same quantities for the indenter. For diamond, $E_i = 1141$ GPa and $\nu_i = 0.07$.^{19–21}

Microscratch as well as friction and wear tests were carried out using a CETR microtribometer (CETR Inc.). In the microscratch tests, a conical diamond indenter having a tip radius of 1.5 μm and an included angle of 60° was drawn over the sample surface, and the load was ramped up until substantial damage occurred. An acoustic emission sensor was used to detect crack formation during scratching. The 1-mm long scratches were made by translating the sample while ramping the loads on the conical tip over different loads ranging from 6 mN to 50 mN. The coefficient of friction, friction force, normal load, and acoustic emission signal were detected *in situ* during scratching. The friction and wear tests were conducted against a WC ball with a 4-mm diameter and surface finish of about 2 nm RMS in reciprocating mode. Typical test conditions were as follows: stroke length 7.0 mm, frequency 0.1 Hz, average linear speed 1.0 mm s^{−1}, normal load 20 mN, temperature 22 ± 1°C, and relative humidity 45 ± 5%. The friction force was measured for a total sliding distance of 5 m.

Scratch and wear tracks were observed using a Philips XL30 field-emission environmental SEM.

RESULTS AND DISCUSSION

Hardness and Elastic Modulus

Representative load–displacement curves and AFM images of indentations made at 5 mN peak indentation load on SiC, CoCrMo, Ti-6Al-4V, and stainless steel are compared in Figure 1. SiC exhibits the lowest indentation depth and highest slope of unloading curve, followed by CoCrMo, stainless steel, and Ti-6Al-4V. The AFM images show the same trend as the load–displacement curves; SiC exhibits the smallest indentation mark, followed by CoCrMo, stainless steel, and Ti-6Al-4V. Pile-up (the indented material around the indenter above its original surface²⁰) was found around the indentation impressions for all samples. As smaller pile-up was observed around the indentation impressions of SiC.

Multiple partial loading/unloading nanoindentations made on SiC, CoCrMo, Ti-6Al-4V, and stainless steel were used to determine their hardness and elastic modulus as a function of depth. The data collected in the tests are displayed in Figure 2, along with hardness and elastic modulus values that were calculated from the load–displacement curves using standard techniques.^{19–21} SiC exhibits the highest hardness of about 45.8 GPa and elastic modulus of about 370 GPa among the samples examined, followed by CoCrMo, stainless steel, and Ti-6Al-4V. The hardness values of stainless steel and Ti-6Al-4V are comparable while the elastic modulus of Ti-6Al-4V is higher than that of stainless steel.

Scratch Resistance

Figure 3 shows the coefficient of friction and acoustic emission profiles as a function of increasing normal load and SEM

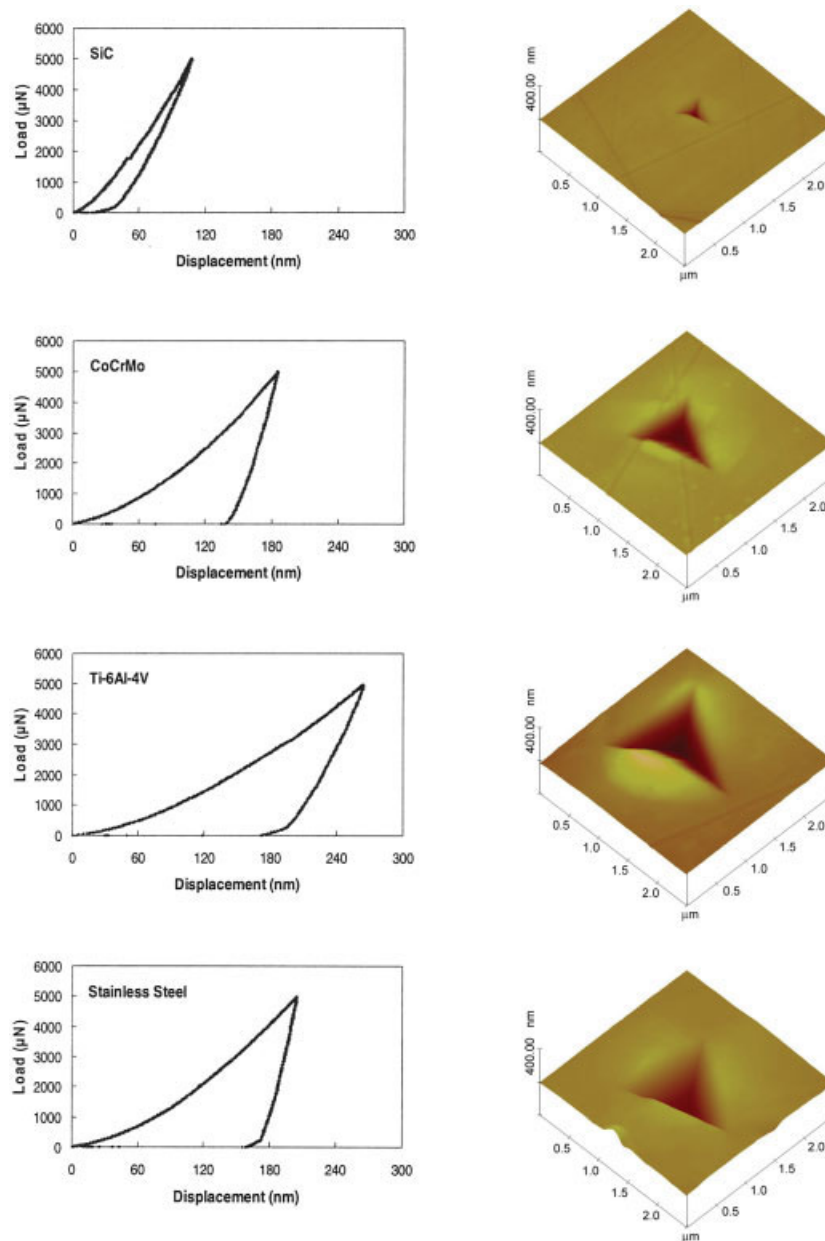


Figure 1. (a) Representative load–displacement curves and (b) AFM images of indentations made at 5 mN peak indentation load on SiC, CoCrMo, Ti-6Al-4V, and stainless steel. [Color figure can be viewed in the online issue, which is available at www.interscience.wiley.com.]

images of three regions over scratches: at the beginning of the scratch (indicated by A on the friction profile), at the point of initiation of damage at which the coefficient of friction increases to a high value or increases abruptly (indicated by B on the friction profile), and towards the end of the scratch (indicated by C on the friction profile), for SiC, CoCrMo, Ti-6Al-4V, and stainless steel. At the initial stages of scratching, SiC exhibits a lower coefficient of friction than other samples. With increasing normal load, the coefficient of friction of SiC remains a constant low value of 0.03 until the normal load reaches the critical load of about 22 mN at which its coefficient of friction rises to 0.1. A corresponding acoustic emission signal was detected at 22 mN, indicating crack

formation. CoCrMo and stainless steel exhibit a continuous increase in the coefficient of friction with increasing normal load before significant damage occurred to the samples while Ti-6Al-4V exhibits a large variation in the coefficient of friction at the beginning of scratch.

The SEM images show that below the critical loads all samples were damaged by plowing, associated with the plastic flow of material. In region A, for SiC, a shallower plowing scratch track was found without any debris on the side of the scratch, which is likely the cause for the lower coefficient of friction before the critical load. For all other samples, in addition to plowing scratch tracks, pile-up and debris particles were found on the sides of the scratches. SiC exhibits the

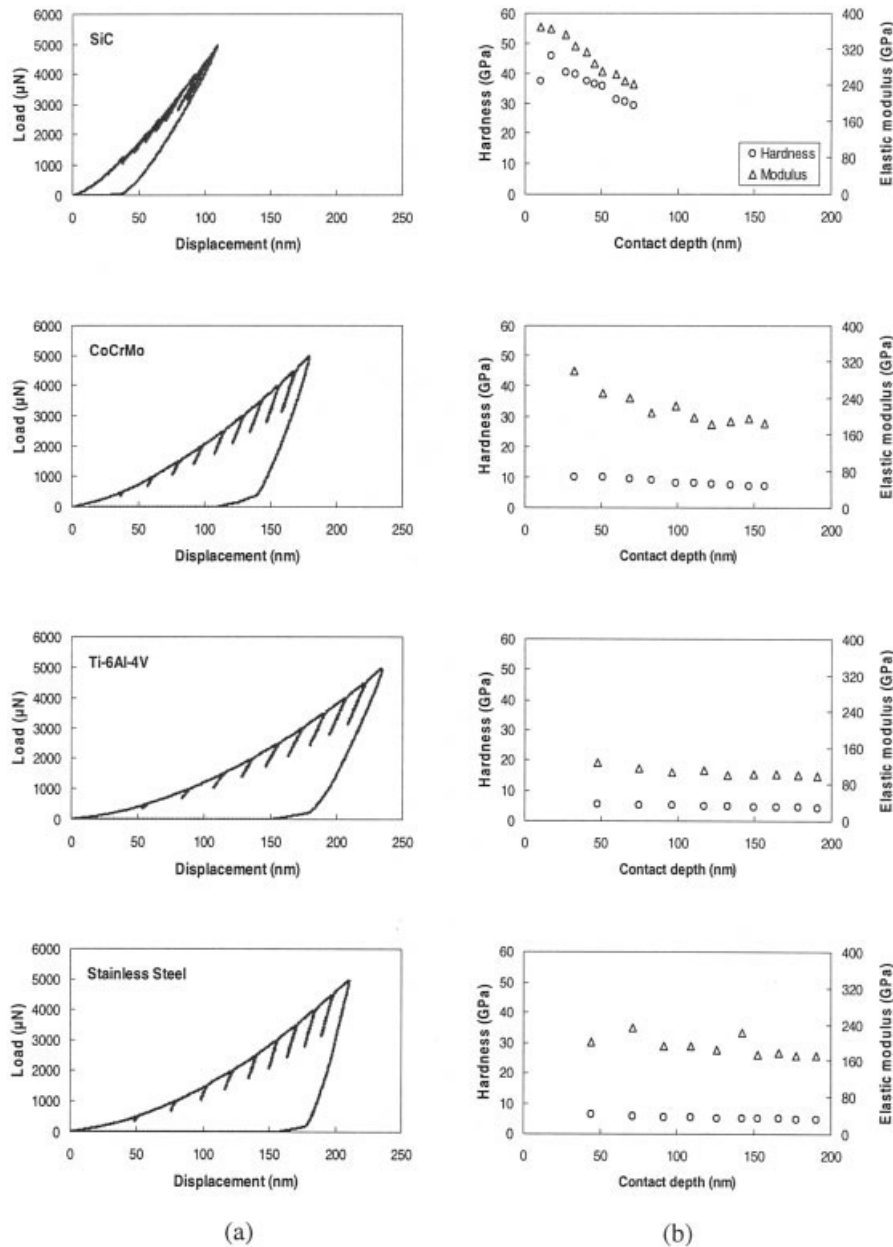


Figure 2. Multiple partial loading/unloading nanoindentations made on SiC, CoCrMo, Ti-6Al-4V, and stainless steel for determining their hardness and elastic modulus as a function of depth.

smallest scratch track among the samples examined, followed by CoCrMo, stainless steel, and Ti-6Al-4V. After the critical load for SiC, cracks and debris particles were found on the side of the scratch from the critical load to the end. The crack formation at/after the critical load is responsible for the detected acoustic emission signals. For all other samples, deep plowing with plastic flow of material and pile-up was observed on the side of the scratch and a curly chip was found at the end of the scratch. This is a typical characteristic of ductile metal alloys. The acoustic emission sensor used in this study is not sensitive to the plastic deformation. This is why no acoustic signals were detected for CoCrMo, stainless steel, and Ti-6Al-4V.

Friction and Wear Resistance

The coefficient of friction as a function of sliding distance for various samples sliding against a WC ball is compared in Figure 4. The SEM images of wear tracks and debris formed on all samples when sliding against a WC ball after a sliding distance of 5 m are compared in Figures 5 and 6. Among the samples examined, SiC exhibits the lowest coefficient of friction, followed by CoCrMo, Ti-6Al-4V, and stainless steel. SiC shows a constant low coefficient of friction of about 0.17 during the sliding. CoCrMo shows an abrupt increase in the coefficient of friction at a sliding distance of 2 m. For Ti-6Al-4V and stainless steel, an abrupt increase in the coeffi-

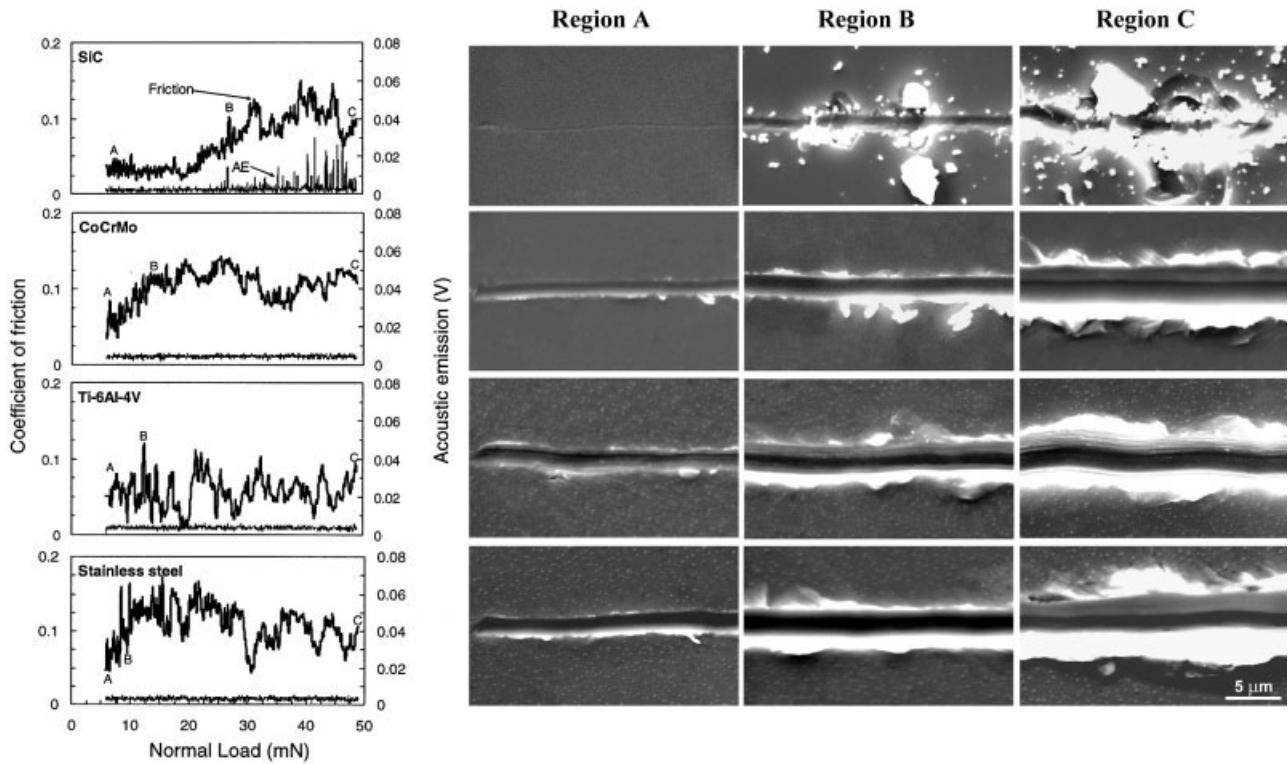


Figure 3. Coefficient of friction and acoustic emission profiles as a function of increasing normal load and SEM images of three regions over scratches: at the beginning of the scratch (indicated by A on the friction profile), at the point of initiation of damage at which the coefficient of friction increases to a high value or increases abruptly (indicated by B on the friction profile), and towards the end of the scratch (indicated by C on the friction profile), for SiC, CoCrMo, Ti-6Al-4V, and stainless steel.

cient of friction was observed right from the beginning of sliding, and then the coefficient of friction remains at higher values compared to SiC and CoCrMo.

The SEM images (Figure 5) show that SiC has the smallest wear track and the least amount of debris, followed by CoCrMo, stainless steel, and Ti-6Al-4V. For Ti-6Al-4V and stainless steel, scratches with plastic flow of material were found within the wear tracks, which is believed to be attrib-

uted to the sudden increase in the coefficient of friction at the beginning of sliding. The amount of debris particles accumulated at the end and on the sides of the wear track of Ti-6Al-4V is at least several times more than those of other samples. SEM images of the debris particles (Figure 6) show that the debris particle size of SiC is the smallest, followed by CoCrMo, Ti-6Al-4V, and stainless steel. The debris particle size is relatively uniform for SiC and CoCrMo. For Ti-6Al-4V and stainless steel, in addition to small debris particles, many large chip-like debris particles were found. The edges of these large chip-like debris particles exhibit plastic deformation tearing characteristics. The large debris particles were, in turn, pulverized into small debris particles by the WC ball during subsequent sliding. These debris particles were severely strain hardened with high contact and shear stresses by the WC ball at the tribological interface. In addition, the debris particles, in particular the large chip-like debris particles, scratched the sample, generating additional sample damage with a higher coefficient of friction.

During wear tests, sample surface experiences shear stress. The maximum wear shear stress locates beneath the sample surface rather than on the sample surface.²⁴ This maximum wear shear stress can result in yielding (plastic deformation) for low strength materials and, consequently, delamination and bulking of the surface layer. Among the four materials tested in this study, the relatively low strength materials are

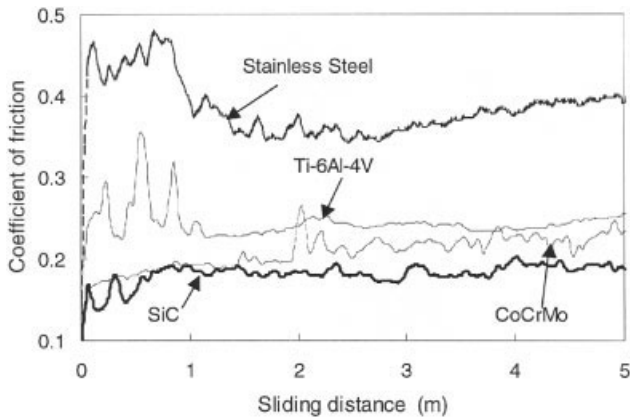


Figure 4. Coefficient of friction as a function of sliding distance for SiC, CoCrMo, Ti-6Al-4V, and stainless steel when slid against a WC ball.

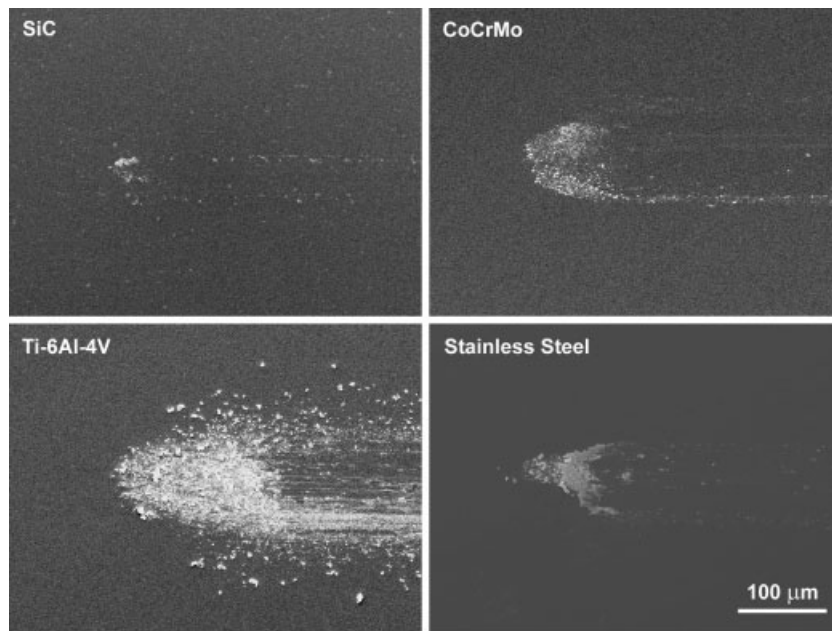


Figure 5. SEM images of wear tracks and debris formed on SiC, CoCrMo, Ti-6Al-4V, and stainless steel when slid against a WC ball after a sliding distance of 5 m. The end of the wear track is on the left-hand side of the image.

Ti-6Al-4V and stainless steel. This may be why large chip-like debris particles were found with Ti-6Al-4V and stainless steel. The higher hardness and elastic modulus of SiC makes

plastic deformation and material flow more difficult. It is well known that wear surfaces of metals and alloys are easily oxidized and contaminated through reactions with environ-

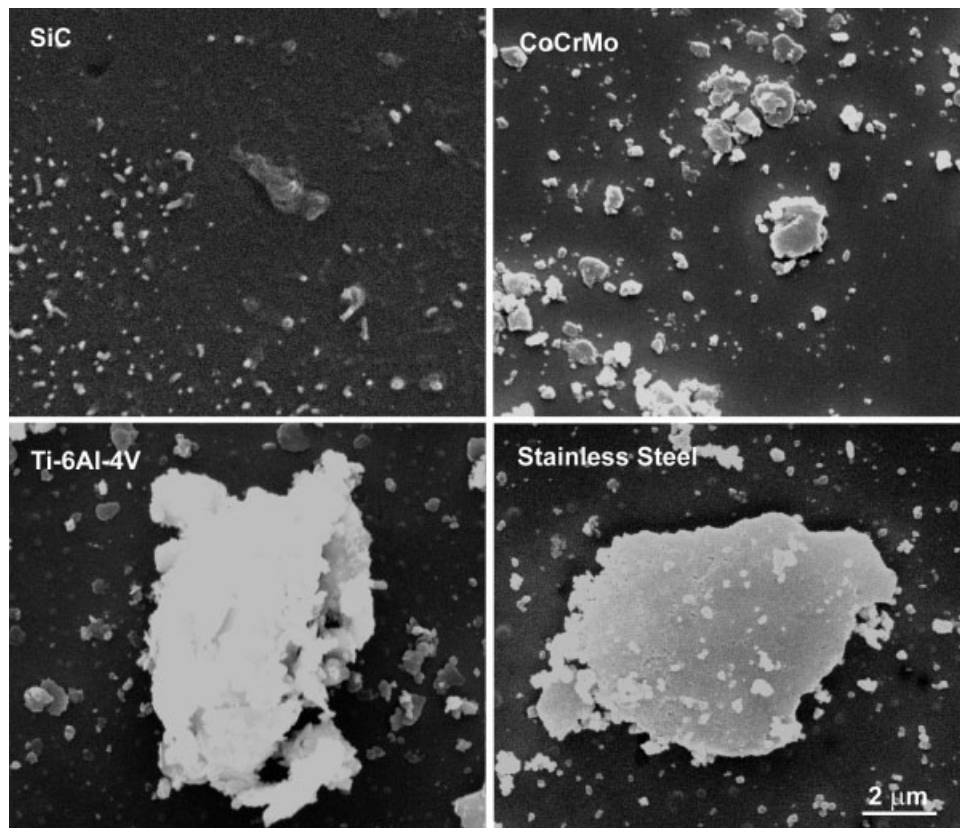


Figure 6. SEM images of wear debris particles formed on SiC, CoCrMo, Ti-6Al-4V, and stainless steel when slid against a WC ball.

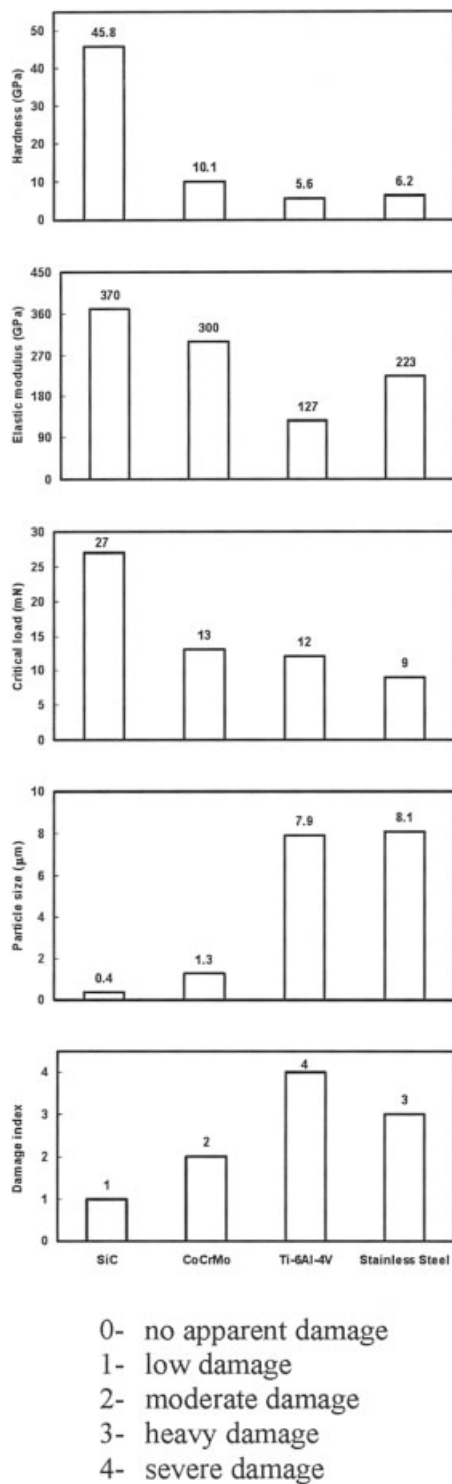


Figure 7. Bar charts summarizing the hardness, elastic modulus, scratch, and wear results of SiC, CoCrMo, Ti-6Al-4V, and stainless steel.

mental elements at the tribological interface. Oxidation and contamination layers are brittle and contribute to the generation of debris particles at the tribological interface. It has been proven that SiC is chemically inert and resistant to harsh mechanical and chemical environments. Without surface ox-

idation or a contamination layer, SiC retained the superior mechanical properties throughout the process. This is believed to be another key contribution to the high wear resistance of SiC.

Figure 7 summarizes the hardness, elastic modulus, scratch, and wear results of SiC, CoCrMo, Ti-6Al-4V, and stainless steel. The damage bar chart in Figure 7 was plotted based on optical image examination of the scratch and wear tracks, as well as, debris after tests: 0 represents no apparent damage; 1, low damage; 2, moderate damage; 3, heavy damage; and 4, severe damage. Good correlation exists between mechanical properties and scratch/wear damage. Higher mechanical properties result in less scratch/wear damage. The currently used metals and alloys such as CoCrMo, Ti-6Al-4V, and stainless steel cannot meet the ever-increasing requirement for better tribological performance in orthopedic applications. SiC has been identified as the superior material due to its better mechanical and tribological properties, and should find more applications in biomedical applications. The advanced coating technology has made it possible to coat SiC on various substrates and retain the same high mechanical and tribological properties.^{15-17,21}

CONCLUSIONS

SiC shows higher hardness, elastic modulus, and scratch resistance, as well as, lower friction than the other materials currently used in orthopedic applications. Compared with CoCrMo, Ti-6Al-4V, and stainless steel, SiC exhibits a low coefficient of friction with fewer and smaller debris particles. A good correlation between mechanical properties and scratch/wear damage was found. Higher hardness and elastic modulus together with the inertness of SiC are attributed to its superior tribological properties. Severe plastic ploughing damage, observed at the beginning of wear sliding, indicates that the currently used metallic orthopedic materials do not provide adequate load-carrying capabilities. The nanoindentation technique together with accelerated scratch, friction, and wear tests used in this article can be satisfactorily used for the characterization of orthopedic materials. SiC has proven to be an exceptional choice as a material for orthopedic applications.

REFERENCES

- Aspenberg P, Anttila A, Kontinen YT, Lappalainen R, Goodman S, Nordsletten L, Santavirta S. Benign response to particles of diamond and SiC: bone chamber studies of new joint replacement coating materials in rabbits. *Biomaterials* 1996;17:807-812.
- Santavirta S, Takagi M, Nordsletten L, Anttila A, Lappalainen R, Kontinen YT. Biocompatibility of silicon carbide in colony formation test in vitro: a promising new ceramic THR implant coating material. *Arch Orthop Trauma Surg* 1998;118:89-91.
- Allen M, Butter R, Chandra L, Lettington A, Rushton N. Toxicity of particulate silicon carbide for macrophages, fibroblasts

- and osteoblast-like cells in vitro. *Biomed Mater Eng* 1995;5: 151–159.
4. Kotzar G, Freas M, Abel P, Fleischman A, Roy S, Zorman C, Moran J, Melzak J. Evaluation of MEMS materials of construction for implantable medical devices. *Biomaterials* 2002;23: 2737–2750.
 5. McLaughlin J, Harris G. SiC for subretinal applications. *Research Accomplishments 2000, National Nanofabrication Users Network*; 2000. p 34–35.
 6. Nordsletten L, Hogasen A, Kontinen Y, Santavirta S, Aspenberg P, Aasen A. Human monocytes stimulation by particles of hydroxyapatite, silicon carbide, and diamond: in vitro studies of new prosthesis coatings. *Biomaterials* 1996;17:1521–1527.
 7. Monnink S, van Boven A, Peels H, Tigchelaar I, de Kam P, Crijns H, van Oeveren W. Silicon carbide coated coronary stents have low platelet and leukocyte adhesion during platelet activation. *J Invest Med* 1999;47:304–310.
 8. Kalnins U, Erglis A, Dinne I, Kumsars I, Jegere S. Clinical outcomes of silicon carbide coated stents in patients with coronary artery disease. *Med Sci Monit* 2002;8:PI16–PI20.
 9. McGee MA, Howie DW, Costi K, Haynes DR, Wildenauer CI, Percy MJ, McLean JD. Implant retrieval studies of the wear and loosening of prosthetic joints: a review. *Wear* 2000;241: 158–165.
 10. Friedman RJ, An YH, Jiang M, Draughn RA, Bauer TW. In vivo mechanical and histological evaluation of bone ingrowth and apposition to metal implants of different surface textures in the rabbit femur. *J Orthop Res* 1996;14:455–464.
 11. Bessette B, Fassler F, Tanzer M, Brooks C. Total hip arthroplasty in patients younger than 21 years: a minimum 10 year follow-up. *Can J Surg* 2003;46:257–262.
 12. Lemons J, Freese H. Metallic biomaterials for surgical implant devices. *BONEZone* 2002; Fall.
 13. Goodman SB, Lind M, Song Y, Smith RL. In vitro, in vivo, and tissue retrieval studies on particulate debris. *Clin Orthop* 1998; 352:25–34.
 14. Kadoya Y, Kobayashi A, Ohashi H. Wear and osteolysis in total joint replacements. *Acta Orthop Scand Suppl* 1998;278:1–16.
 15. Li X, Bhushan B. Micro/nanomechanical characterization of ceramic films for microdevices. *Thin Solid Films* 1999;340: 210–217.
 16. Bhushan B, Sundararajan S, Li X, Zorman CA, Mehregany M. Micro/nanotribological studies of single-crystal silicon and polysilicon and SiC films for use in MEMS devices. In: Bhushan B, editor. *Tribology issues and opportunities in MEMS*. Netherlands: Kluwer Academic; 1998. p 407–430.
 17. Li X, Bhushan B, Takashima K, Baek CW, Kim YK. Mechanical characterization of micro/nanoscale structures for MEMS/NEMS applications using nanoindentation techniques. *Ultramicroscopy* 2003;97:481–494.
 18. Cherednichenko DI, Drachev RV, Sudarshan TS. Self-congruent process of SiC growth by physical vapor transport. *J Crystal Growth* 2004;262:175–181.
 19. Bhushan B, Li X. Nanomechanical characterization of solid surfaces and thin films (invited). *Int Mater Rev* 2003;48:125–164.
 20. Li X, Bhushan B. A review of nanoindentation continuous stiffness measurement technique and its applications. *Mater Character* 2002;48:11–36.
 21. Bhushan B, Li X. Nanomechanical characterization of ceramic materials. In: Gogotsi Y, Domnich V, editors. *High pressure surface science and engineering*. Bristol: IOP Publishing; 2003. p 321–348.
 22. Oliver WC; Pharr GM. An improved technique for determining hardness and elastic-modulus using load and displacement sensing indentation experiments. *J Mater Res* 1992;7:1564–1583.
 23. Sneddon IN. The relation between load and penetration in the axisymmetric boussinesq problem for a punch of arbitrary profile. *Int J Eng Sci* 1965;3:47–56.
 24. Bhushan B. *Principles and applications of tribology*. New York: Wiley; 1999.